Nanoscale

PAPER

View Article Online
View Journal | View Issue

Cite this: *Nanoscale*, 2017, **9**, 5329

Multi-step encapsulation of chemotherapy and gene silencing agents in functionalized mesoporous silica nanoparticles†

Jianliang Shen, ‡[a,b] Haoran Liu,‡[b,c] Chaofeng Mu,[b] Joy Wolfram,[b] Wei Zhang,[a] Han-Cheon Kim,[b] Guixian Zhu,[b] Zhongbo Hu,[c] Liang-Nian Ji,[a] Xuewu Liu,[b] Mauro Ferrari,[b,d] Zong-Wan Mao *[a] and Haifa Shen*[b,e]

Received 16th January 2017,
Accepted 16th March 2017

DOI: 10.1039/c7nr00377c

rsc.li/nanoscale

Drug to carrier ratio is an important consideration in designing drug platforms, since a low loading capacity necessitates the use of high doses of carriers, which can result in side effects. Here, we have engineered a platform to co-deliver small molecule drugs and small interfering RNA (siRNA). This platform consists of cyclodextrin-grafted polyethylenimine (CP) functionalized mesoporous silica nanoparticles (MSNP). A unique multi-step encapsulation procedure was used to obtain a high loading capacity for doxorubicin (DOX) and siRNA oligos specific for the PKM2 gene that encodes pyruvate kinase M2, an enzyme catalyzing the final rate-limiting step in glycolysis. We systematically characterized this platform (CP-MSNP@DOX/PKM2) *in vitro* and evaluated its therapeutic efficacy *in vivo* with a mouse model of triple negative breast cancer (TNBC). Exposure of TNBC cells to CP-MSNP@DOX/PKM2 resulted in suppressed target gene expression, reduced cell proliferation, and enhanced apoptosis. Intravenous administration of the drug substantially decreased the tumor burden in comparison to DOX or siRNA monotherapy. In conclusion, we have developed a platform for efficient co-delivery of small molecule drugs and therapeutic siRNA.

Introduction

In the past three decades, numerous studies have demonstrated that nanotechnology is a powerful tool for cancer therapy.[1–3] Various functional nanomaterials have been designed for the delivery of therapeutic agents, such as small molecule drugs, nucleic acids, peptides, and proteins.[4–6] The use of nanocarriers usually leads to increased therapeutic efficacy and fewer side effects, due to reduced renal clearance, prolonged blood circulation, and improved tumor accumulation.[6–10] Some of the most widely studied nanocarriers include liposomes, polymeric nanoparticles, metal nanoparticles, mesoporous silica nanoparticles (MSNPs), and nanoporous silicon particles.[11–17] Among these delivery platforms, MSNPs have attracted attention owing to their large pore volume and surface area, good biocompatibility, easily functionalized surface, and high cellular uptake efficiency.[18–21] Many studies have focused on the modification of MSNPs for effective drug delivery and gene transfection.[22–27] However, the drug loading capacity of these particles is limited, since drug loading is confined to the nanopores of MSNPs. Moreover, the prevalence of drug resistance necessitates the use of higher drug doses.[28] Therefore, treatment usually requires multiple rounds of particle administration, which is an inconvenience for clinical translation. Another consequence of reduced loading capacity is the requirement to use high quantities of delivery vehicles in a single administration, which can result in toxicity due to poor metabolism, minimal elimination, and activation of the immune system. Thus, strategies are needed to enhance the drug loading capacity of drug delivery vehicles.

According to the World Cancer Report, cancer remains a major cause of mortality worldwide.[29] Notably, the metabolism of cancer cells differs substantially from that of normal cells, and alterations in normal metabolism are fundamental for cancer cell growth and survival.[30,31] Therefore, the combi-

[a]*MOE Laboratory of Bioinorganic and Synthetic Chemistry, School of Chemistry and Chemical Engineering, Sun Yat-sen University, Guangzhou 510275, China. E-mail: cesmzw@mail.sysu.edu.cn*
[b]*Department of Nanomedicine, Houston Methodist Hospital Research Institute, Houston 77030, USA. E-mail: hshen@houstonmethodist.org*
[c]*College of Materials Science and Opto-Electronic Technology, University of Chinese Academy of Sciences, Beijing 100049, China*
[d]*Department of Medicine, Weill Cornell Medicine, New York 10065, USA*
[e]*Department of Cell and Developmental Biology, Weill Cornell Medicine, New York 10065, USA*

†Electronic supplementary information (ESI) available. See DOI: 10.1039/c7nr00377c

‡These authors contributed equally to this work.

nation of chemotherapy with agents that target cancer metabolism holds promise for improving cancer therapy.[32,33] Small interfering RNA (siRNA) is an efficient technology to down-regulate genes involved in cancer cell metabolism.[34,35] Pyruvate kinase M2 (PKM2), a key gene in cancer cell metabolism, plays an important role in metabolic reprogramming and cell cycle progression.[36,37] Notably, PKM2 is overexpressed in most breast cancer cells and has been found to desensitize cells to chemotherapeutic agents.[38–40] Therefore, suppression of PKM2 has the potential to improve the efficacy of chemotherapy.[41]

In this study, we have developed a functional MSNP delivery platform for PKM2 siRNA and doxorubicin (DOX) combination therapy. As shown in Scheme 1, a two-step loading process has been developed to achieve high drug-loading capacity. The first step involves the loading of DOX inside the pores of the MSNP, while the second step entails the capture of DOX in the hydrophobic cavities of cyclodextrin (CD), which has been conjugated to the surface of MSNPs. Specifically, MSNPs were functionalized with CD-grafted polyethylenimine (CP). In addition to providing a secondary reservoir for DOX, the high positive charge density of CP facilitated PKM2 siRNA loading through electrostatic interactions. The anticancer activity of the CP-MSNP@DOX/siRNA system was evaluated in an orthotopic triple negative breast cancer (TNBC) model. TNBC usually displays aggressive characteristics and has limited treatment options due to a lack of receptor targets.[42–44]

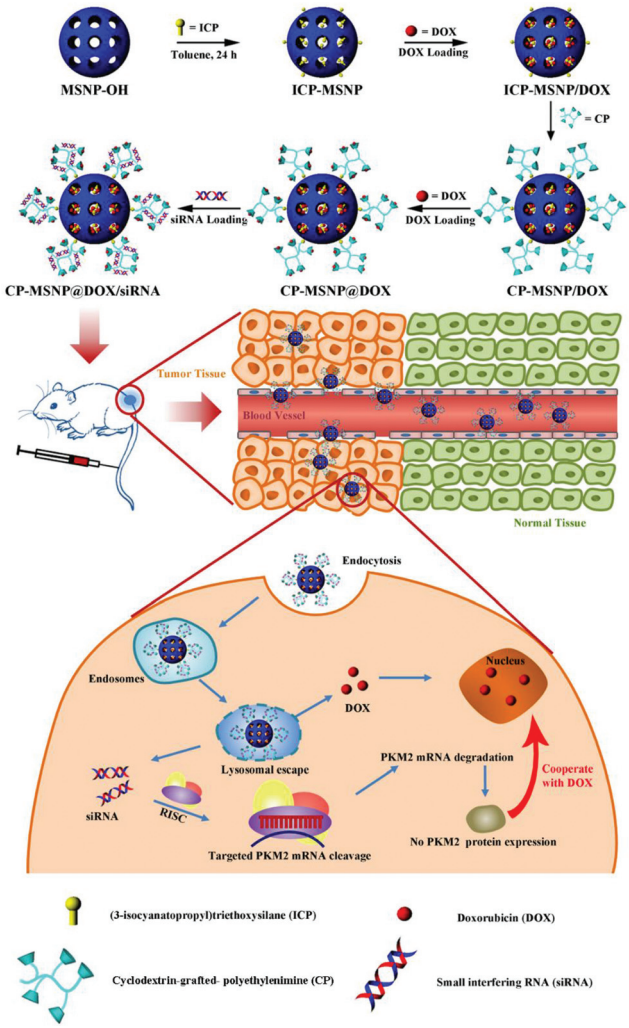

Scheme 1 Schematic representation of the fabrication of cyclodextrin-grafted polyethylenimine-mesoporous silica nanoparticles@doxorubicin/small interfering RNA (CP-MSNP@DOX/siRNA) as a codelivery system for triple-negative breast cancer (TNBC). ICP, (3-isocyanatopropyl)triethoxysilane.

Experimental section

General materials

All starting reagents were purchased from Sigma-Aldrich and used without additional treatment unless otherwise indicated. Other materials were acquired from the following sources: DOX, triethylamine, branched PEI (MW 1.8 kDa), β-cyclodextrin, *N*-cetyltrimethylammonium bromide (CTAB), tetraethoxysilane (TEOS), 4′,6-diamidino-2-phenylindole (DAPI), 3-isocyanatopropyltriethoxysilane (ICP), scrambled (Scr) siRNA, and PKM2 siRNA from Sigma-Aldrich; BSA-Alexa Fluor 647 conjugate, Alexa Fluor 647 phalloidin, propidium iodide (PI), Dulbecco's modified Eagle's medium (DMEM) high glucose, and fetal bovine serum (FBS) from Thermo Fisher Scientific; LysoTracker Green from Invitrogen; SYTOX Blue and Annexin V-Alexa Fluor®647 from BD Biosciences; siRNA^{FAM}, AF647 siRNA from Qiagen; antibodies from Cell Signaling Technology. PKM2 siRNA sense and anti-sense sequences were CCAUAAUCGUCCUCACCAA[dT][dT] and UUGGUGAGGACGAU UAUGG[dT][dT], respectively.

Cell lines

MDA-MB-231 cells were obtained from ATCC (Rockville, MD). Cells were cultured in DMEM supplemented with 10% FBS and 1% penicillin–streptomycin solution and maintained at 37 °C with 5% CO_2.

Preparation of β-cyclodextrin-grafted PEI (CP)

Beta-cyclodextrin-grafted PEI was synthesized as previously reported.[23] Briefly, 6-mono-tosylated cyclodextrin (65 mg, 0.05 mmol) was added dropwise into a solution containing PEI (12 mg, 0.093 mmol) and triethylamine (4.72 mg, 0.047 mmol) in dimethyl sulfoxide (DMSO, 3 ml). The reaction was allowed to proceed at 70 °C in a nitrogen atmosphere for three days. The resulting mixture was dialyzed against water in a Spectra/Por MWCO 1000 bag and then separated with a Sephadex-G25 column.

Synthesis and characterization of ICP-MSNP/DOX, CP-MSNP/DOX, and CP-MSNP@DOX

Fabrication of MSNP was carried out as previously reported.[23] MSNP-OH was synthesized by mixing TEOS with CTAB in a basic aqueous solution. Excess CTAB was removed by suspending MSNP-OH in a solution containing methanol/hydrochloric

acid (20/1, v/v) for 24 h. The particles were then centrifuged (12 000 rpm, 10 min), resuspended in anhydrous toluene (1 g, 80 mL), and mixed with ICP (0.25 mL, 1.0 mmol). The reaction was allowed to proceed for 24 h to yield ICP-MSNP.

DOX loading into the pores of ICP-MSNP to yield ICP-MSNP/DOX was performed according to a modified version of a previously reported protocol.[25] Briefly, ICP-MSNP (1 mg) was added to a DOX solution (2 ml, 4.5 mg mL^{-1}) in MeOH/H_2O (3 : 5, v/v) at pH 7.4 and sonicated (5 min) to obtain a well-dispersed suspension that was further stirred for 12 h at room temperature. Next, the particles were centrifuged (12 000 rpm, 10 min) and sonication (1 min) was used to re-disperse the pellet in phosphate buffered saline (PBS; 5 mL). The suspension was then added to CP (100 mg) in ethanol solution. The reaction between the amino groups of CP and the functional groups of ICP was allowed to proceed for 20 h at 20 °C to obtain CP-MSNP/DOX. The resulting product was centrifuged (12 000 rpm, 10 min) and washed thoroughly with ethanol and methanol to remove free ICP and CP prior to overnight vacuum drying.

To obtain CP-MSNP@DOX, DOX was loaded into the hydrophobic cavities of cyclodextrin according to a previously reported protocol.[56] Briefly, the pellet of CP-MSNP/DOX (1 mg) was dispersed in PBS, sonicated (1 min), and mixed with DOX (3 mg) for 12 h at room temperature. The resultant suspension was then centrifuged (12 000 rpm, 10 min) and the pellet was redispersed in PBS. This centrifugation–redispersion cycle was repeated three times to remove free DOX. The final product was vacuum dried overnight and stored at 4 °C.

Drug loading capacity was calculated as shown below:

$$\text{Drug loading capacity } (\%) = W_t/W_s \times 100\%,$$

where W_t represents the weight of DOX loaded into the nanoparticles and W_s represents the nanoparticle weight after vacuum drying.

The size and morphology of the CP-MSNP@DOX carrier was determined with transmission electron microscopy (TEM; Tecnal G2 20 S-TWIN, FEI Company, Hillsboro, OR). The sample was prepared by adding CP-MSNP@DOX solution (10 μL) onto a carbon-coated copper grid. The sample was stained with phosphotungstic acid hydrate (2%), washed three times in distilled water, and air-dried. Ultraviolet–visible (UV/Vis) spectra was recorded in the wavelength range of 250–750 nm using a DU® 730 UV-Vis spectrophotometer. The zeta potential and size of the particles were determined with a Nano-ZS Zetasizer (Malvern, Worcestershire, UK) using the DTS (nano) program. CP-MSNP@DOX nanoparticles were mixed with $siRNA^{FAM}$ at a ratio of 60 : 1 (w/w) in HEPES buffer and dropped on the surface of a microscope slide. The slides were covered with a coverslip and images were captured using a Fluoview TM 1000 confocal microscope (Olympus). CP-MSNP@DOX (100 μL) was added to a serum solution consisting of FBS/PBS (v/v = 1 : 1, 1 mL). The resulting mixture was incubated at 37 °C and stirred with an electronic stirrer (500 rmp) to mimic conditions in the blood circulation. Samples were collected at set time points and the particle size was determined by dynamic light scattering (DLS) using a Nano-ZS Zetasizer.

At different stages in the functionalization process, the particles were analyzed by Fourier transform infrared spectroscopy (FTIR; Nicolet 6700, Thermo Scientific, USA). N_2 adsorption–desorption isotherms were recorded on an Autosorb iQ analyzer (Quantachrome, USA). The samples were degassed at 100 °C for 12 h. The surface area was calculated from the low-pressure adsorption data using the Brunauer Emmett Teller (BET) model and the pore size was determined using the density functional theory (DFT) model. Thermogravimetric (TGA) analysis of powder samples was recorded at a heating rate of 10 °C min^{-1} from 25 °C to 600 °C under airflow using a TGA Q500 (TA Instruments). Moreover, solid-state ^{13}C and ^{29}Si cross polarization magic angle spinning (CP-MAS) solid-state nuclear magnetic resonance (SSNMR) spectra were obtained using a Bruker MSL300 spectrometer equipped with a 4 mm Bruker MAS rotor.

Optimization of CP-MSNP@DOX/siRNA

CP-MSNP and CP-MSNP@DOX were mixed with Scr siRNA in 2-[4-(2-hydroxyethyl)piperazin-1-yl]ethanesulfonic acid (HEPES, 10 mM) buffer at various weight ratios (particles/siRNA: 20 : 1, 40 : 1, 60 : 1, 80 : 1, 100 : 1), and incubated for 15 min at 4 °C. Electrophoresis was performed on a 2% agarose gel to determine the binding efficiency of siRNA to CP-MSNP or CP-MSNP@DOX. Electrophoresis was carried out at a constant voltage of 120 V for 20 min in TAE running buffer (2 M Tris, 250 mM sodium acetate, 50 mM EDTA, pH 7.8). siRNA bands were stained with ethidium bromide and visualized with a ChemiDoc XRS+ UV transilluminator (Bio-Rad). The zeta potential of the particles was measured as described above. All other studies were performed with particles that had a particle/siRNA ratio of 60 : 1 (w/w).

For confocal microscopy studies, CP-MSNP@DOX was mixed with $siRNA^{FAM}$ in HEPES buffer and placed on the surface of a microscope slide. The slide was covered with a coverslip and images were captured using a Fluoview TM 1000 confocal microscope (Olympus).

To demonstrate that exposure to sodium dodecyl sulfate (SDS) caused the siRNA to disassociate from the particles, electrophoresis was performed as described above. CP-MSNP/siRNA and CP-MSNP@DOX/siRNA were incubated with 1% SDS solution for 30 min prior to performing electrophoresis.

siRNA protection against ribonuclease (RNase) and serum

To evaluate whether CP-MSNP and CP-MSNP@DOX could protect siRNA from degradation, siRNA (0.2 μg) was loaded into CP-MSNP and CP-MSNP@DOX. The particles were exposed to RNase (1 μg, 1 μL) at 37 °C for 1 h. The enzyme was then inactivated with ethylenediaminetetraacetic acid (EDTA, 0.25 M). The particles were dissolved in NaOH and SDS was used to release the siRNA from CP. Electrophoresis was performed as described above.

Naked Scr siRNA and CP-MSNP@DOX/Scr siRNA were incubated in 50% FBS at 37 °C. Samples were collected after

30 min, 6 h, 12 h, 24 h, 48 h, and 60 h, and immediately mixed with gel loading buffer containing 1% SDS. Electrophoresis was performed as described above.

In vitro drug release

The release of DOX and siRNA from CP-MSNP@DOX/siRNA^{FAM} was measured in HEPES buffer (10 mM) at pH 5.0 or pH 7.4. At various time points, the particles were centrifuged (10 min, 12 000 rpm) and the supernatant was collected for analysis. The fluorescence intensity of the supernatant was measured with a Synergy H4 hybrid microplate reader (Biotek).

Cellular internalization of CP-MSNP@DOX/siRNA

The intracellular accumulation of CP-MSNP@DOX/siRNA^{FAM} was evaluated using flow cytometry, confocal microscopy, and TEM. For flow cytometry analysis, MDA-MB-231 cells were seeded overnight in 6-well plates at a density of 3×10^5 cells per well. The cells were then incubated with CP-MSNP@DOX/siRNA^{FAM} (siRNA: 50 nM). Samples were collected after 2 h, 6 h, and 24 h, and washed three times with FBS solution (2%). The intracellular accumulation of siRNA^{FAM} and DOX was determined using a LSRII Flow Cytometer (BD Bioscience). For confocal microscopy studies, MDA-MB-231 cells were seeded overnight in 2-well chamber slides at a density of 5×10^4 cells per well. The cells were then exposed to CP-MSNP@DOX/siRNA^{FAM} (siRNA: 50 nM) and confocal microscopy images were captured after 2 h, 4 h and 6 h. Cell nuclei were labeled with 4′,6-diamidino-2-phenylindole (DAPI). For TEM studies, MDA-MB-231 cells were seeded overnight in 6-well plates at a density of 3×10^5 cells per well. The cells were treated with CP-MSNP@DOX/siRNA (50 μg mL^{-1} or 100 μg mL^{-1}) for 2 h. The cells were then collected and fixed overnight at 4 °C in PBS containing 2.5% glutaraldehyde. Subsequently, the cells were treated with osmium tetroxide, stained with uranyl acetate and lead citrate, and visualized with a JEM-100CX TEM (JEOL).

Intracellular trafficking of CP-MSNP@DOX/siRNA

MDA-MB-231 cells were seeded overnight in 2-well chamber slides at a density of 5×10^4 cells per well. The cells were then incubated with CP-MSNP@DOX/AF647 siRNA (siRNA: 50 nM) for 0.5 h, 2 h, and 6 h. Cells were harvested and fixed with paraformaldehyde (4%). Subsequently, cells were blocked with BSA (1%) in PBS containing Tween-20 (0.1%; PBST) and stained with LysoTracker Green, DAPI, and Alexa Fluor 647 Phalloidin. Confocal microscopy images were captured using a FluoView TM 1000 (Olympus) confocal microscope.

Cell viability

The *in vitro* toxicity of empty CP-MSNP, CP-MSNP/Scr, CP-MSNP@DOX, CP-MSNP@DOX/Scr siRNA (siRNA: 10–100 nM), and CP-MSNP@DOX/PKM2 siRNA (siRNA: 10 nM) was evaluated using a MTT-based colorimetric assay (Sigma-Aldrich) according to the manufacturer's instructions. Cells were seeded overnight in 96-well plates at a density of 5×10^3 cells per well. The cells were then treated with nanoparticles for 48 h or 72 h.

Cell cycle analysis

MDA-MB-231 cells were seeded overnight at a density of 5×10^5 cells per well in 6-well plates. Cells were then treated with PBS, CP-MSNP, CP-MSNP@DOX, CP-MSNP@DOX/Scr siRNA (siRNA: 10 nM), or CP-MSNP@DOX/PKM2 siRNA (siRNA, 10 nM) for 48 h, trypsinized, washed, and fixed with alcohol (70%) on ice for 2 h. Next, the fixed cells were stained with PI staining solution (50 μg mL^{-1} PI, 1 mg mL^{-1} RNase A, and 0.05% Triton X-100) for 30 min at 37 °C in the dark. For each sample, 10^4 cells were analyzed using a LSRII Flow Cytometer (BD Bioscience).

Cell apoptosis

Cell apoptosis was assessed with flow cytometry using the Annexin V-Alexa Fluor®647 apoptosis detection kit I (BD Biosciences) according to the manufacturer's instructions. MDA-MB-231 cells were seeded overnight in 6-well plates at a density of 5×10^5 cells per well. The cells were then exposed to PBS, CP-MSNP, CP-MSNP@DOX, CP-MSNP@DOX/Scr siRNA (siRNA: 10 nM), or CP-MSNP@DOX/PKM2 siRNA (siRNA, 10 nM) for 48 h, trypsinized, and stained with annexin V-AF647 (2.5 μL) and SYTOX Blue (2.5 μL) for 30 min at 37 °C. For each sample, 10^4 cells were analyzed using a LSRII Flow Cytometer (BD Bioscience, USA).

For western blot analysis, cells were seeded overnight in 6-well plates at a density of 5×10^5 cells per well. Cells were then exposed to PBS, CP-MSNP, CP-MSNP@DOX, CP-MSNP@DOX/Scr siRNA (siRNA: 10 nM), or CP-MSNP@DOX/PKM2 siRNA (siRNA: 10 nM) for 48 h and lysed using the M-PER protein extraction reagent (Pierce Inc., USA). The protein samples were separated on a 4–20% gel with SDS-polyacrylamide gel electrophoresis (PAGE) and transferred to a nitrocellulose membrane (Bio-Rad Inc., USA). A rabbit anti-human cleaved PARP antibody (Cell Signaling) was used at a dilution of 1 : 1000. β-Actin was used as a loading control. For western blot analysis of tumor samples, athymic nude mice (4–6 weeks; Charles River) were inoculated with MDA-MB-231 cancer cells in the mammary fat pad (2×10^6 cells per mouse). When the mean tumor volume reached 150–200 mm^3, mice were divided into five groups and treated once a week for four weeks with PBS, CP-MSNP (900 μg per mouse per week), CP-MSNP@DOX (900 μg per mouse per week), CP-MSNP@DOX/Scr siRNA (15 μg siRNA per mouse per week), or CP-MSNP@DOX/PKM2 siRNA (siRNA: 15 μg per mouse per week). Mice were sacrificed three days after the last treatment and tumor samples were collected. Western blot analysis was performed as described above.

Gene silencing *in vitro*

For western blot analysis, MDA-MB-231 cells were seeded overnight in 6-well plates at a density of 2×10^5 cells per well. The cells were then incubated with CP-MSNP@DOX/siRNA (siRNA: 10 nM) for 48 h. Western blot analysis was performed as described above using a PKM2 antibody (Cell Signaling, 1 : 1000). The ratio of PKM2 to β-actin was calculated based on densitometric quantification.

ATP levels *in vitro*

MDA-MB-231 cells were seeded overnight in 6-well plates at a density of 2×10^5 cells per well. Cells were then incubated with CP-MSNP, CP-MSNP/siRNA (Scr and PKM2: 50 nM) for 48 h. Subsequently, the cells were collected and lysed using an adenosine 5′-triphosphate (ATP)-release buffer (Sigma, Gillingham, UK). ATP levels were quantified with an ATP bioluminescent somatic cell assay kit (Sigma-Aldrich) according to the manufacturer's instructions. Values were normalized to the total protein content in the cell lysates.

Biodistribution of CP-MSNP@DOX/siRNA *in vivo*

All of the experimental procedures in the animal studies were approved by the Institutional Animal Care and Use Committee at the Houston Methodist Research Institute. For the biodistribution studies, female athymic nude mice (4–6 weeks; Charles River) were inoculated with MDA-MB-231 tumor cells in the mammary fat pad (2×10^6 cells per mouse). Studies were initiated when the mean tumor volume reached 150–200 mm^3. In order to visualize the tumor vasculature, mice were intravenously administered with BSA-Alexa Fluor 647. CP-MSNP@DOX/$siRNA^{FAM}$ (siRNA: 15 μg per mouse) particles were intravenously administered and videos and images were captured 30 min post-injection with a RS200 TM intravital microscope (Newport). Major organs (heart, liver, spleen, lung, kidney) and tumors were collected 2 h and 24 h post-injection. Fluorescent images of the tissues were captured using the IVIS 200 spectrum *in vivo* preclinical imaging system (PerkinElmer) ($n = 3$). In addition, major organs (heart, liver, spleen, lung, kidney) and tumors were collected for inductively coupled plasma atomic emission spectroscopy (ICP-AES) analysis of silicon content using a 720-ES ICP Optical Emission Spectrometer (Varian). Briefly, the weights of the organs were recorded and the tissues were homogenized (Tissue Homogenizer, Omni International) and digested in an ethanol (20%) and NaOH (1 N) solution (3 ml) for 72 h at room temperature. The extracts were centrifuged (4200 rpm, 25 min) and the supernatant (0.5 mL) was diluted in deionized water (2.5 mL) for analysis. A Fluka Silicon Standard for ICP (Sigma Aldrich) was used to create a standard curve.

Evaluation of safety and therapeutic efficacy *in vivo*

To determine the therapeutic efficacy of CP-MSNP@DOX/PKM2 siRNA *in vivo*, athymic nude mice were inoculated with MDA-MB-231 cancer cells in the mammary fat pad (2×10^6 cells per mouse). When the mean tumor volume reached 150–200 mm^3, mice were divided into five groups and treated once a week for four weeks with PBS, CP-MSNP (900 μg per mouse per week), CP-MSNP@DOX (900 μg per mouse per week), CP-MSNP@DOX/Scr siRNA (siRNA: 15 μg per mouse per week), or CP-MSNP@DOX/PKM2 siRNA (siRNA: 15 μg per mouse per week) ($n = 3$). The tumor volume was calculated using the following formula: tumor volume = $0.5 \times \text{width}^2 \times$ length. Mice were sacrificed three days after the last treatment and tumor samples were collected, fixed with 4% paraformaldehyde overnight, and embedded in paraffin for analysis. DNA fragmentation was analyzed with a terminal deoxynucleotidyl transferase dUTP nick end labeling (TUNEL) assay (Maxin-Bio) according to the manufacturer's instructions. A Ki-67 antibody (Abcam, 1 : 100) was used for immunohistochemical staining of proliferating cells, while PKM2 was stained with a PKM2 antibody (Cell Signaling, 1 : 200) according to the manufacturer's instructions. Additionally, major organs (liver, spleen, kidney, lung, brain, and heart) were fixed in formalin, embedded in paraffin, sectioned (4 μm), and stained with hematoxylin and eosin (H&E) staining. Tissue sections were analyzed for leukocyte infiltration, cell death, and other signs of organ damage. At least five random sections from each slide were examined.

Statistical analysis

Statistical analysis was performed with the Student's *t*-test. Differences were considered statistically significant at $P < 0.05$ (*) and $P < 0.01$ (**).

Results and discussion

Fabrication and characterization of CP-MSNP@DOX

The fabrication and characterization of CP-MSNP is outlined in the materials and methods section and was reported in detail in our previous study.[23] The fabrication process for CP-MSNP@DOX is illustrated in Scheme 1. Briefly, oxidized silica particles were modified with ICP to generate a negative charge that would improve DOX encapsulation and minimize premature drug release (Fig. S1†).[24,25,45] Following DOX encapsulation inside the silica pores (ICP-MSNP/DOX), CP was conjugated to the particles and DOX was loaded within the hydrophobic cavities of cyclodextrin (CP-MSNP@DOX). Finally, binding of siRNA to CP occurred through electrostatic interactions.

The functionalization of MSNP-OH with CP was confirmed with ^{13}C and ^{29}Si CP-MAS SSNMR spectroscopy (Fig. 1a). The results suggest that: (i) the signal resonating at 170 ppm corresponds to the characteristic peak of the amide carbonyl carbon (C4) and amide carbons of PEI, (ii) the signals resonating between 50 ppm and 85 ppm represent the characteristic peaks of the cyclodextrin skeleton, and (iii) the signals resonating between 10 ppm and 50 ppm are attributed to the characteristic carbon peaks on the ICP linker. Additionally, the two silicon peaks at −55 ppm and −110 ppm in the ^{29}Si CP-MAS SSNMR spectrum of CP-MSNP (Fig. 1b) most likely correspond to functionalized silica (T region) and bulk silica (Q region), respectively. The CP-MAS SSNMR results from this study and those previously reported by Zhao *et al.*[19] provided strong evidence for successful CP functionalization of the particles. Furthermore, TGA analysis revealed that the weight percentage of ICP and CP on the MSNP was 11% and 16%, respectively (Fig. 1c). The surface area and pore size of the MSNP at various steps in the functionalization process was measured with BET and DFT analysis, respectively (Fig. 1d and e). A decrease in the surface area and pore size of ICP-MSNP/DOX compared to

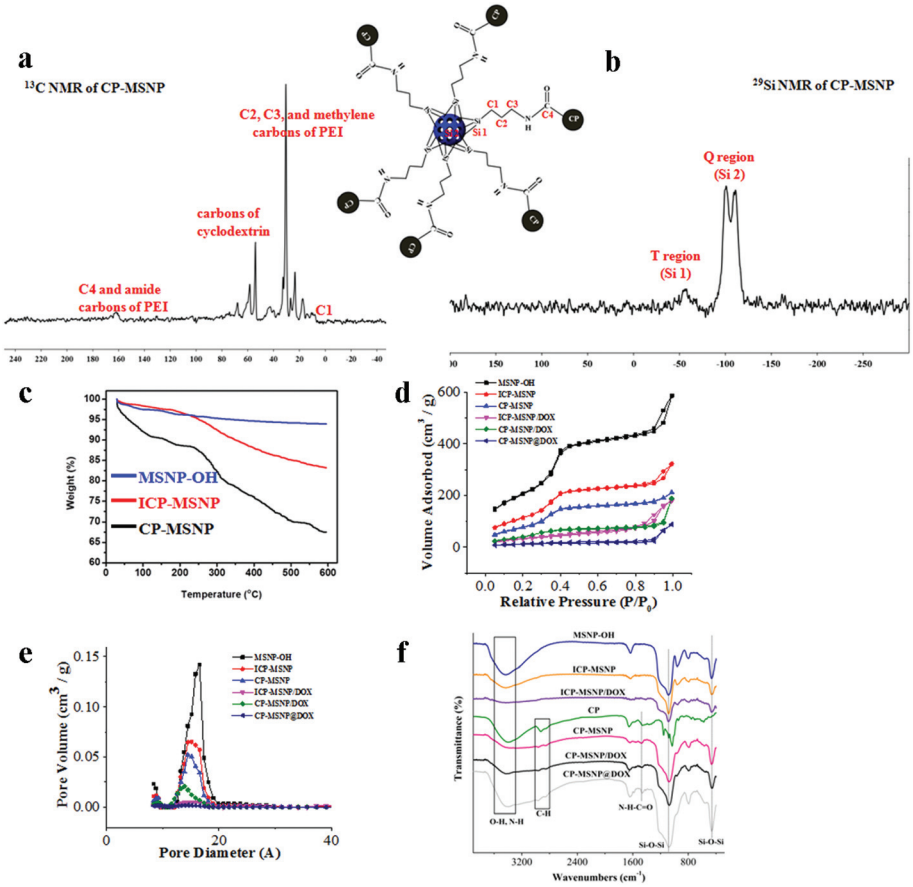

Fig. 1 Characterization of the delivery system. (a) ^{13}C cross polarization magic angle spinning (CP-MAS) solid-state nuclear magnetic resonance (SSNMR) spectrum of cyclodextrin-grafted polyethylenimine (CP)-MSNP. (b) ^{29}Si CP-MAS SSNMR spectrum of CP-MSNP. (c) Thermogravimetric analysis (TGA) of MSNP-OH, ICP-MSNP and CP-MSNP at a heating rate of 10 °C min^{-1} from 25 °C to 600 °C under airflow. (d) Brunauer–Emmett–Teller (BET) nitrogen adsorption/desorption isotherms and (e) density function theory (DFT) pore size distribution of MSNP-OH, ICP-MSNP, CP-MSNP, ICP-MSNP/DOX, CP-MSNP/DOX, and CP-MSNP@DOX. (f) Fourier transform infrared spectroscopy (FTIR) spectrum of CP, MSNP-OH, ICP-MSNP, CP-MSNP, ICP-MSNP/DOX, CP-MSNPDOX, and CP-MSNP@DOX. DOX, doxorubicin; ICP, (3-isocyanatopropyl)triethoxysilane.

ICP-MSNP indicates that DOX was successfully loaded inside the pores during the first encapsulation step. Upon modification of ICP-MSNP/DOX with CP, the pore diameter was approximately 0.65 nm, which is similar to that of free β-cycoldextrin. Subsequent loading of DOX in CP reduced the pore size to ~0 nm, suggesting that the second encapsulation step was successful (Fig. 1d and e). Moreover, results obtained with FTIR spectroscopy were in accordance with the other characterization studies and with previously reported results (Fig. 1f).[23] In conclusion, the above-mentioned studies provide evidence for CP functionalization and multi-step encapsulation of DOX.

TEM, DLS, and laser Doppler electrophoresis were used to measure the size and zeta potential of the CP-MSNP@DOX. As shown in Fig. 2a, TEM images demonstrate that the particles have a mesoporous structure. Moreover, DLS analysis revealed that the CP-MSNP@DOX and CP-MSNP@DOX/siRNA had an average size of 103.25 ± 3.56 nm and 101 ± 4.22 nm, respectively (Fig. 2b). These results indicate that particle size is unaffected by siRNA binding. Changes in the surface chemistry of the particles were confirmed by monitoring the zeta potential throughout the fabrication process (Fig. 2c). For instance, the conjugation of CP changed the zeta potential from negative to positive, thereby enabling siRNA binding through electrostatic interactions. Notably, DOX encapsulation inside the silica pores and the cyclodextrin cavities did not change the zeta potential (Fig. 2c).

As shown in Fig. 2d, the two-step DOX encapsulation process increased the overall loading capacity, as was evident from color changes that occurred in the sample. Likewise, absorbance measurements (DOX absorption peak: 495 nm) of ICP-MSNP/DOX and CP-MSNP@DOX confirmed that two-step encapsulation increased drug loading (Fig. 2e). Specifically, the loading capacity of ICP-MSNP/DOX and CP-MSNP@DOX was 7.3% and 17.8%, respectively. Confocal microscopy was used to visualize siRNA^{FAM} loading in CP-MSNP@DOX, and colocalization of siRNA and DOX suggested successful loading (Fig. 2f). Moreover, the stability of CP-MSNP@DOX in a FBS/PBS solution (v/v = 1 : 1) was monitored over 72 h. The results demonstrate that the particle size remains constant upon prolonged exposure to biomolecules (Fig. 2g).

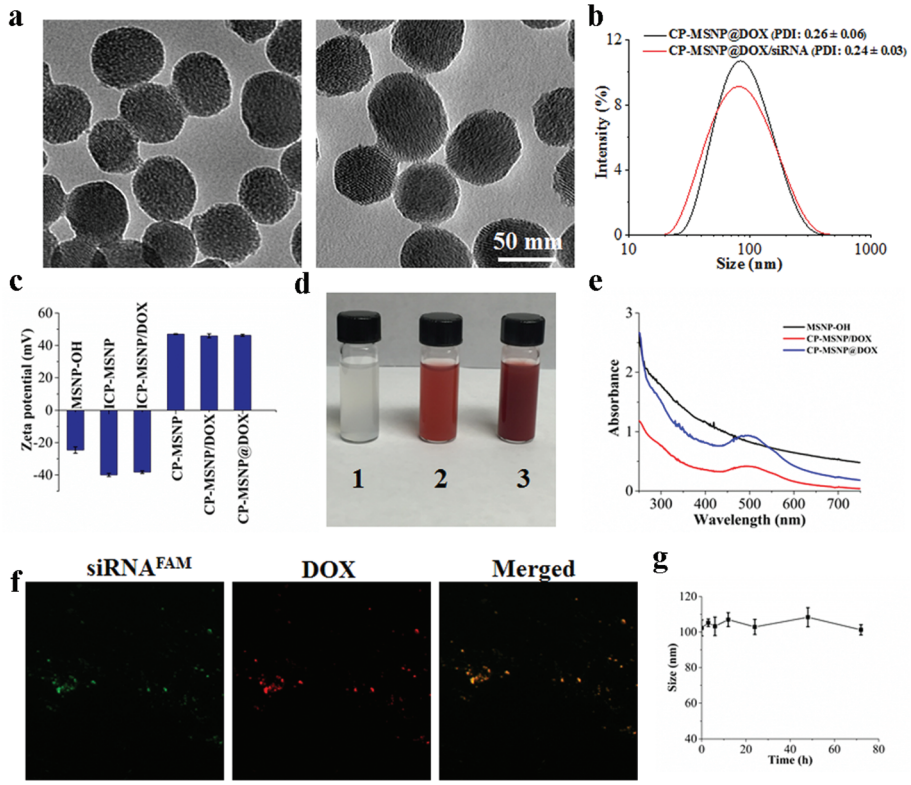

Fig. 2 Characterization of CP-MSNP@DOX/siRNA as a codelivery system for chemotherapeutics and gene silencing agents. (a) Transmission electron microscopy (TEM) images of CP-MSNP@DOX (left panel) and CP-MSNP@DOX/siRNA (right panel). (b) Size distribution of CP-MSNP@DOX and CP-MSNP@DOX/siRNA measured by dynamic light scattering (DLS). (c) Zeta potential of particles at various stages in the fabrication process measured by laser Doppler electrophoresis. Results are presented as the mean ± s.d. of five measurements. (d) Color changes: MSNP-OH (1), CP-MSNP/DOX (2), and CP-MSNP@DOX (3). (e) Ultraviolet–visible (UV-Vis) spectra of MSNP-OH, CP-MSNP/DOX, and CP-MSNP@DOX. (f) Confocal microscopy images of CP-MSNP@DOX/siRNA^{FAM}. DOX, red; siRNA^{FAM}, green. Scale bar, 20 μm. (g) Size of CP-MSNP@DOX in 50% fetal bovine serum (FBS). Results are presented as the mean ± s.d. of three measurements. PDI, polydispersity index.

Optimization of CP-MSNP@DOX/siRNA and release kinetics

In our previous study, we optimized the CP-MSNP to siRNA ratio in regards to siRNA binding affinity, stability, protection ability, and release.[23] However, since DOX was added to the delivery system, new optimization studies were carried out. Agarose gel electrophoresis was performed in order to determine the siRNA condensing ability and binding affinity of CP-MSNP and CP-MSNP@DOX. A wide range of CP-MSNP and CP-MSNP@DOX to siRNA weight ratios (20 : 1 to 100 : 1) were assessed. As shown in Fig. 3a, siRNA was tightly bound to the carrier when the particle to siRNA ratio was above 40 : 1. Moreover, the surface charge of the delivery system ranged from approximately −24.35 mV to +37.38 mV as the particle to siRNA ratio increased (Fig. 3b). Notably, differences in siRNA binding and zeta potential could not be observed between CP-MSNP/siRNA and CP-MSNP@DOX/siRNA, suggesting that DOX encapsulation did not interfere with siRNA loading. Particles with a particle to siRNA weight ratio of 60 : 1 had a moderate positive charge (+8 mV). This ratio was used in further studies, since particles with a strong positive charge can trigger toxicity, while particles with a negative charge generally display lower transfection efficiencies.[46]

The ability of the delivery vehicle to protect siRNA from degradation by RNases was assessed by electrophoresis. SDS was used to release siRNA from the delivery vehicle (Fig. 3c). Exposure to RNase caused degradation of naked siRNA, while siRNA loaded in CP-MSNP or CP-MSNP@DOX remained intact (Fig. 3d). Moreover, the stability of siRNA in the CP-MSNP@DOX delivery system was evaluated over time in a FBS/PBS (v/v = 50/50) solution at 37 °C. After 60 h, a siRNA band could still be detected by electrophoresis (Fig. S2†). On the contrary, our previous studies have shown that naked siRNA degrades after 12 h under identical conditions.[23] Taken together, these results indicate that CP-MSNP@DOX is able to protect siRNA against RNases and serum proteins.

Another important aspect of a delivery vehicle is the rate of drug release.[47] Here, the release of fluorescent siRNA and DOX from CP-MSNP@DOX/siRNA at pH 5.2 and pH 7.4 was evaluated. After 72 h of incubation, the cumulative siRNA release was 60% and 30% at pH 5.5 and pH 7.4, respectively (Fig. 3e). Similarly, 80% of DOX was released after 72 h at pH 5.2, while the corresponding value was 10% at pH 7.4 (Fig. 3e). Higher rates of DOX release under acidic conditions is likely due to the protonation of amine groups in PEI, which increases the positive charge of the carrier, leading to electrostatic repulsion of DOX.[48] It is possible

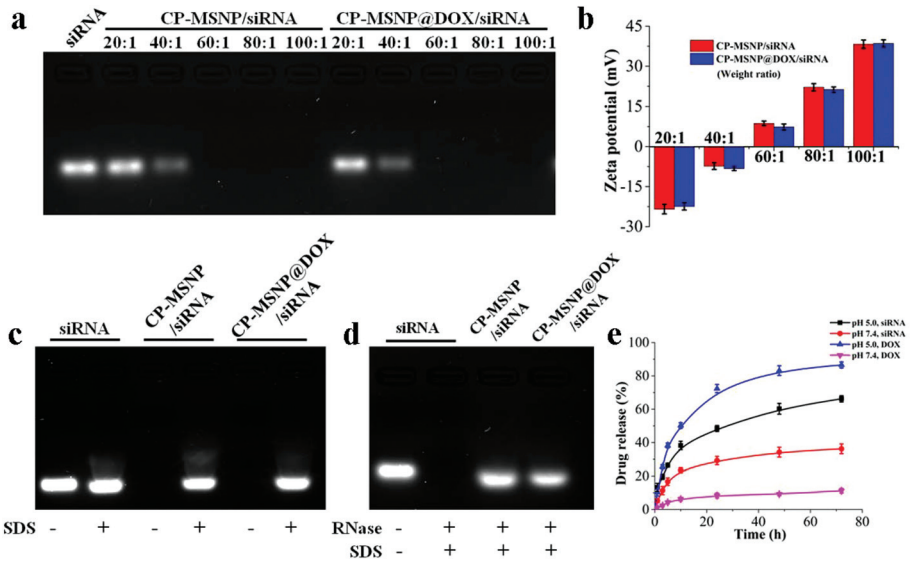

Fig. 3 Optimization of CP-MSNP@DOX/siRNA and drug release kinetics. (a) Agarose gel retardation assay of siRNA loaded in CP-MSNP and CP-MSNP@DOX at various particle to siRNA weight ratios (20 : 1–100 : 1). Naked siRNA was used as a control. (b) Zeta potential of CP-MSNP/siRNA and CP-MSNP@DOX/siRNA with various particle to siRNA weight ratios (20 : 1–100 : 1) measured by laser Doppler electrophoresis. Results are presented as mean ± s.d. of five measurements. (c) Agarose gel retardation assay of siRNA release from CP-MSNP and CP-MSNP@DOX following sodium dodecyl sulfate (SDS) treatment. (d) Agarose gel retardation assay of siRNA protection from RNase degradation. siRNA was dissociated from CP-MSNP and CP-MSNP@DOX using SDS. Naked siRNA was used as a control. (e) Release profiles of DOX and siRNA^{FAM} from CP-MSNP@DOX (particle to siRNA weight ratio, 60 : 1). Particles were incubated in 10% FBS at pH 5.0 or pH 7.4 and the fluorescent intensity of the supernatant was measured. Results are presented as the mean ± s.d. of three measurements.

that free DOX promotes the release of siRNA through electrostatic attraction, since DOX is positively charged in acidic environments. Notably, pH-sensitive release can be exploited for cancer therapy, since tumors have lower pH levels.[48] In essence, accelerated drug release in the tumor microenvironment will cause cancer cells to be exposed to higher drug doses than healthy cells.

Cellular internalization of CP-MSNP@DOX/siRNA

Prior to studying the intracellular uptake of the particles, the biocompatibility of CP-MSNP and CP-MSNP/Scr siRNA was evaluated in MDA-MB-231 cells using an MTT assay. The cell viability was over 90% upon exposure to high concentrations of

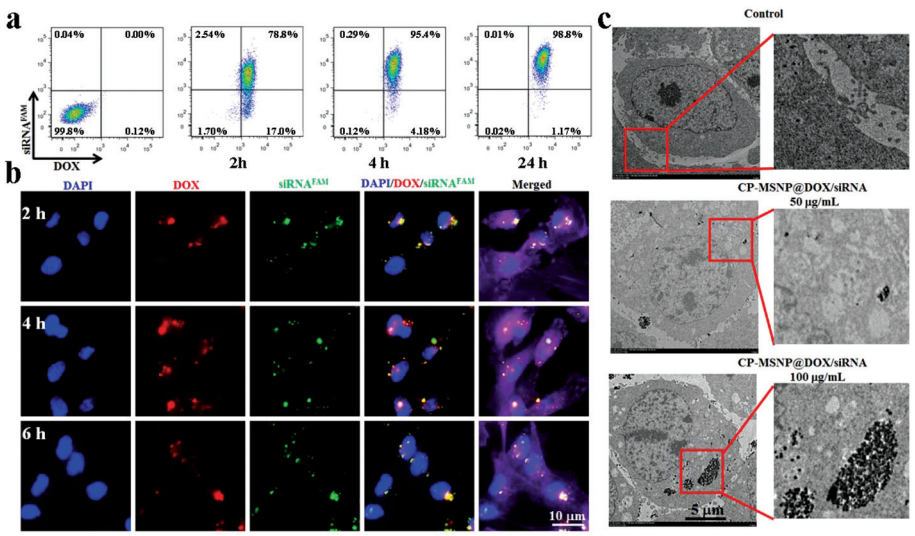

Fig. 4 Cellular internalization of CP-MSNP@DOX/siRNA in MDA-MB-231 breast cancer cells. (a) Quantitative flow cytometry analysis of DOX and siRNA^{FAM} positive cells incubated with CP-MSNP@DOX/siRNA^{FAM} for 2 h, 4 h, or 24 h. Untreated cells were used as a negative control. (b) Confocal images of CP-MSNP@DOX/siRNA^{FAM} in MDA-MB-231 cells. DAPI, blue; DOX, red; siRNA, green; phalloidin, purple. siRNA, 50 nM. (c) TEM images of MDA-MB-231 breast cancer cells treated with CPMSNP@DOX/siRNA for 2 h. Control cells were not treated with particles.

particles (100 μg mL^{-1}) and Scr siRNA (100 nM) (Fig. S3†), indicating a lack of toxicity. Efficient intracellular delivery of hydrophobic drugs and siRNA is a key factor for achieving therapeutic efficacy. The cellular uptake of CP-MSNP@DOX/$siRNA^{FAM}$ was evaluated in MDA-MB-231 human breast cancer cells. Flow cytometry was used to measure cellular uptake of $siRNA^{FAM}$ and DOX at various time points. The percentage of cells that had internalized CP-MSNP@DOX/$siRNA^{FAM}$ was 78.8% (2 h), 95.4% (6 h), and 98.8% (24 h) (Fig. 4a). Confocal microscopy was also used to monitor the intercellular accumulation of siRNA and DOX at different time points (Fig. 4b). Furthermore, the internalization of CP-MSNP@DOX/siRNA by MDA-MB-231 cells was investigated with TEM. As shown in Fig. 4c, the particles accumulated in vesicles in the cytoplasm in a dose-dependent manner. This observation suggests that the cells internalize the nanoparticles through endocytosis, which is consistent with the findings from flow cytometry and confocal microscopy. Taken together, the flow cytometry, confocal microscopy, and TEM results suggest that the platform can effectively overcome challenges associated with the intracellular delivery of siRNA.

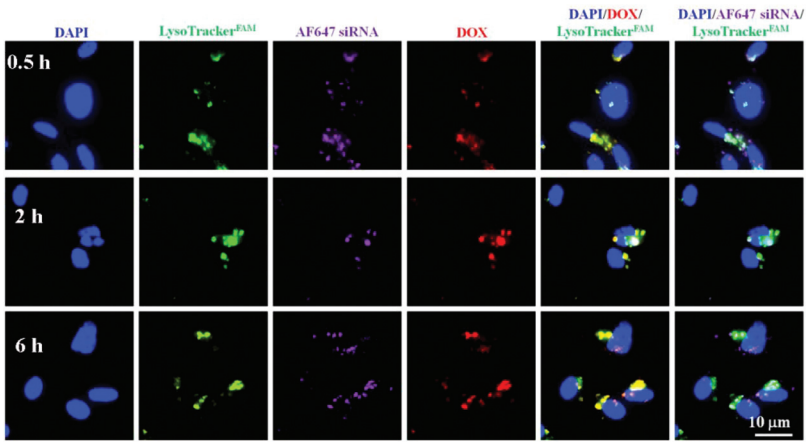

Fig. 5 Intracellular trafficking of CP-MSNP@DOX/AF647 siRNA in MDA-MB-231 breast cancer cells (DAPI, blue; LysoTracker, green; siRNA, purple; DOX, red).

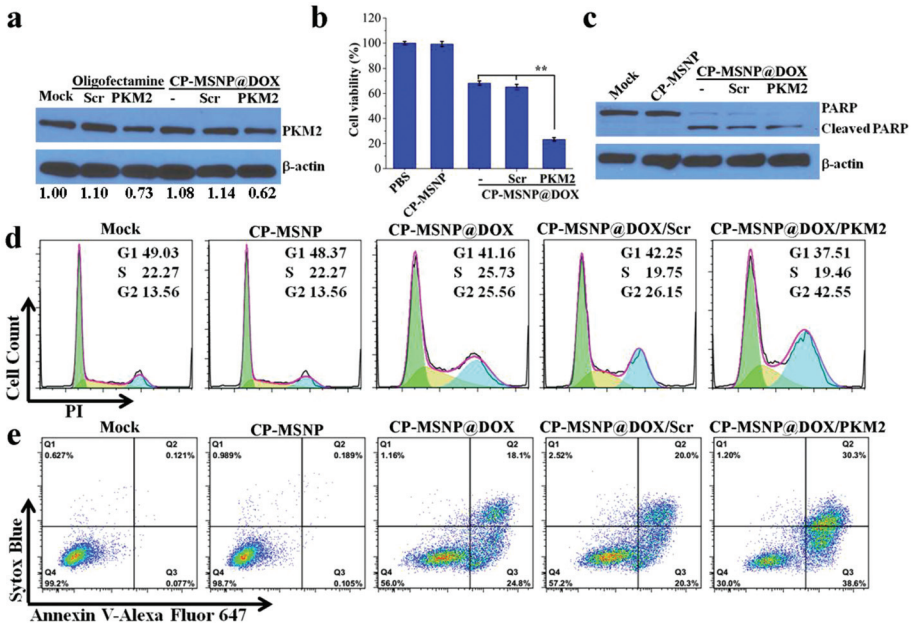

Fig. 6 Anticancer activity of CP-MSNP@DOX, CP-MSNP@DOX/scrambled (Scr) siRNA, and CP-MSNP@DOX/PKM2 siRNA *in vitro*. Cells were incubated with particles for 48 h. siRNA, 20 nM. (a) Western blot analysis of PKM2 protein expression in MDA-MB-231 cells. β-Actin was used as a loading control. Densitometric quantification of PKM2 relative to β-actin was performed and values were normalized to those of control cells. (b) Viability of MDA-MB-231 breast cancer cells (MTT assay). Results are presented as mean ± s.d. of triplicates. **, $P < 0.01$. (c) Western blot analysis of poly ADP ribose polymerase (PARP) and cleaved PARP protein expression. β-Actin was used as a loading control. (d) Flow cytometry of propidium iodide (PI)-labeled cells. (e) Flow cytometry of annexin V-Alexa Fluor 647 and Sytox BlueR labeled cells. PKM2, PKM2 siRNA; Scr, scrambled siRNA.

Intracellular trafficking of CP-MSNP@DOX/siRNA

After confirming that CP-MSNP@DOX/siRNA could efficiently cross the cell membrane, intracellular tracking of the carrier was performed. Notably, endosomal/lysosomal escape of chemotherapeutics and gene silencing agents is essential for therapeutic activity.[49] The intracellular location of CP-MSNP@DOX/AF647 siRNA was determined with confocal microscopy, while acidic endosomes/lysosomes were stained with LysoTracker Green. As shown in Fig. 5, both DOX and siRNA reached the endosomes/lysosomes after 30 min, while maximum levels of colocalization could be observed after 2 h. After 6 h, some of DOX and siRNA were present in the cytoplasm and nucleus, suggesting that the particles had successfully escaped from endosomes/lysosomes. The probable mechanism for lysosomal escape is PEI-induced lysosomal membrane damage, caused by the proton sponge effect or other proposed mechanisms.[16,50]

Evaluation of the anticancer efficacy of CP-MSNP@DOX/siRNA *in vitro*

Previously, we demonstrated that the CP-MSNP/PKM2 siRNA carrier could efficiently downregulate the expression of PKM2, thereby suppressing cell migration, invasion, and tumor growth.[23] Here, we have evaluated the gene silencing efficiency of the CP-MSNP@DOX/PKM2 siRNA carrier in MDA-MB-231 breast cancer cells. Treatment with this carrier caused a reduction in PKM2 protein expression compared to treatment with CP-MSNP@DOX/Scr siRNA (Fig. 6a). In fact, the transfection efficiency of the CP-MSNP@DOX delivery vehicle was slightly higher than that of the commercial transfection reagent Oligofectamine (Fig. 6a). Next, the effect of the carrier on cell proliferation was evaluated in MDA-MB-231 cells using an MTT assay. CP-MSNP@DOX caused a ~30% reduction in cell viability, while the corresponding value for CP-MSNP@DOX/PKM2 siRNA was ~80% (Fig. 6b). These results suggest that PKM2 siRNA sensitizes cells to DOX. Indeed, PKM2-mediated chemosensitization has previously been correlated with reduced levels of adenosine triphosphate (ATP).[32,33] As shown in Fig. S4,† the levels of ATP in MDA-MB-231 cells decrease upon exposure to PKM2 siRNA. In addition to reducing the energy reservoir of the cell, ATP depletion may promote cell death by affecting the balance between pro-apoptotic and anti-apoptotic molecules. In fact, it has been found that ATP levels correlate with the Bax/Bcl-2 ratio in lung cancer cells.[51] To further assess the anticancer activity of the nanoparticles, the cell cycle and key regulators of apoptotic pathways were studied. As shown in Fig. 6c, western blot analysis demonstrated that the treatment resulted in a reduction in the levels of poly (ADP-ribose) polymerase (PARP), which is a well-known substrate in apoptotic signaling.[52] Moreover, flow cytometry was performed to analyze cell cycle phases and apoptosis. In MDA-MB-231 cells treated with CP-MSNP@DOX/PKM2 siRNA, 42.55% of the cell population was arrested in the G2 phase, while 25.56% and 26.15% of cells were in this phase following treatment with CP-MSNP@DOX and CP-MSNP@DOX/Scr siRNA, respectively (Fig. 6d). The ability of CP-MSNP@DOX/PKM2 siRNA to induce apoptosis was studied by staining cells with SYTOX Blue and Annexin V-Alexa Fluor 647. Staining cells with both of these markers makes it possible to distinguish various stages of cellular apoptosis. Early apoptotic cells are generally Annexin V-Alexa Fluor®647 positive and SYTOX Blue negative, while late apoptotic cells are typically double positive. As shown in Fig. 6e, CP-MSNP@DOX, CP-MSNP@DOX/Scr siRNA, and CP-MSNP@DOX/PKM2 siRNA caused 42.9%, 40.3%, and 69.1%, of cells to undergo apoptosis, respectively. Moreover, the combination therapy group had the greatest number of late apoptotic cells. The ability of CP-MSNP@DOX/PKM2 siRNA to arrest cells in the G2 phase and induce apoptosis is a clear indication of their anticancer activity. It should be noted that the treatment might also induce other forms of cell death, since it is difficult to distinguish late apoptotic cells from necrotic cells. In fact, glucose deprivation has previously been shown to induce necrosis in cancer cells.[53]

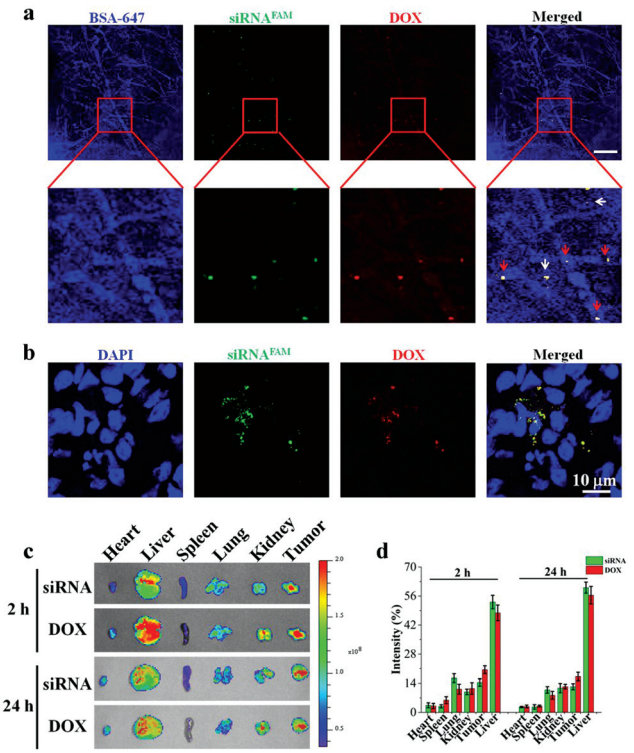

Fig. 7 Tumor accumulation and biodistribution of CP-MSNP@DOX/siRNA^{FAM} in athymic nude mice bearing orthotopic MDA-MB-231 breast cancer tumors. (a) Intravital microscopy images captured 30 min post-injection of CP-MSNP@DOX/siRNA^{FAM} (yellow). Tumor blood vessels are displayed in blue (bovine serum albumin Alexa Fluor 647 conjugate). Red arrows, particles in the tumor vasculature; white arrows, particles in the tumor interstitium. Scale bar, 200 μm. (b) Confocal microscopy images of tumors 30 min post-injection of CP-MSNP@DOX/siRNA^{FAM}. DAPI, blue. (c) Fluorescent images of major organs (heart, liver, spleen, kidneys and lungs) and tumors captured with the IVIS spectrum *in vivo* pre-clinical imaging system. (d) Quantitative analysis of fluorescent images captured with the IVIS system. Results are presented as mean ± s.d. (n = 3) of the total detected fluorescence signal.

Biodistribution of CP-MSNP@DOX/siRNA

The tumor accumulation of intravenously injected CP-MSNP@DOX/siRNA^{FAM} was studied in an orthotopic mouse model of MDA-MB-231 breast cancer. Intravital microscopy was used to capture videos and images of particle accumulation in tumor tissue. The vasculature was visualized using a bovine serum albumin (BSA) Alexa Fluor 647 conjugate (Fig. S5†). As shown in Fig. 7a, CP-MSNP@DOX/siRNA^{FAM} nanoparticles were successfully delivered to the tumor site 30 min post-injection. Notably, while most of the particles were present in the tumor vasculature, some were visible in the tumor interstitium. Real-time particle flow in tumor vasculature can be seen in ESI Video 1.† Confocal microscopy images confirm that the particles were present in the tumors 30 min post-injection (Fig. 7b). These results demonstrate that CP-MSNP@DOX/siRNA rapidly accumulates in tumor tissue following intravenous administration. Next, major organs, including the heart, liver, spleen, lungs, and kidneys, were visualized 2 h and 24 h after particle administration using an IVIS-200 imaging system (Fig. 7c). The liver displayed the highest fluorescence intensity, which is typical for nanoparticle biodistribution studies.[54] Quantitative analysis of the images demonstrated that 12% of the detected siRNA and 16% of the detected DOX deposited in tumors 24 h after injection (Fig. 7d). The tumor accumulation of nanoparticles is usually increased compared to small molecules due to the EPR effect.[55] In summary, the results suggest that this drug delivery system can successfully deliver siRNA and DOX to tumor tissue.

CP-MSNP@DOX/siRNA-induced suppression of tumor growth

The therapeutic efficacy of CP-MSNP@DOX/PKM2 siRNA was assessed in an orthotopic model of MDA-MB-231 breast cancer. As illustrated in Fig. 8a, treatment with CP-MSNP@DOX/PKM2 siRNA was more effective at inhibiting tumor growth compared to treatment with MSNP@DOX. Moreover, combination therapy resulted in an almost threefold decrease in the tumor weight compared to monotherapy (Fig. 8b). Furthermore, western blot analysis of tumor tissues was performed to confirm siRNA-mediated suppression of PKM2 expression (Fig. 8c). Additionally, western blot results demonstrated decreased levels of PARP and increased levels of cleaved PARP in tumor samples from mice treated with DOX or siRNA (Fig. 8d). Immunohistochemistry analysis further confirmed suppression of PKM2 expression in tumor tissues from mice treated with CP-MSNP@DOX/PKM2 siRNA (Fig. 8e). In addition, the combination therapy group had the lowest levels of proliferating cancer cells and the highest levels of apoptotic cancer cells as was evident from Ki67 and terminal deoxynucleotidyl transferase mediated dUTP nick end-labeling (TUNEL) staining (Fig. 8e and S6†). Furthermore, repeated injections of particles did not affect the body weight of mice

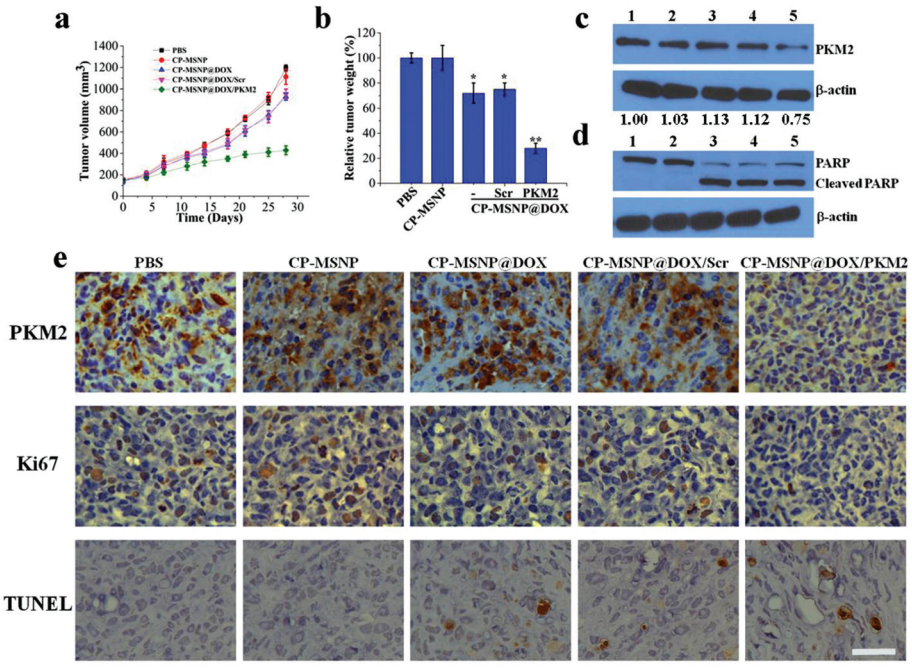

Fig. 8 Anticancer efficacy of CP-MSNP@DOX/siRNA in athymic nude mice bearing orthotopic MDA-MB-231 breast cancer tumors. Mice were intravenously injected once a week for four weeks with PBS, CP-MSNP, CP-MSNP@DOX, CP-MSNP@DOX/Scr siRNA, or CP-MSNP@DOX/PKM2 siRNA. (a) Tumor volume. (b) Tumor weights at the end of the treatment period. Results are presented as mean ± s.d. (n = 3). (c, d) Western blot analysis of PKM2, PAPR, and cleaved PARP levels in tumor samples from mice treated with PBS (1), CP-MSNP (2), CP-MSNP@DOX (3), CP-MSNP@DOX/Scr siRNA (4), or CP-MSNP@DOX/PKM2 siRNA (5). β-Actin was used as a loading control. (e) Immunohistochemical analysis of PKM2, Ki67, and terminal deoxynucleotidyl transferase mediated dUTP nick end-labeling (TUNEL) in tumor tissues (brown staining). *, $P < 0.05$; **, $P < 0.01$. Scale bar, 20 μm. PKM2, PKM2 siRNA; Scr, scrambled siRNA.

(Fig. S7†) or cause gross morphological changes in major organs (Fig. S8†). These results indicate that CP-MSNP@DOX/PKM2 siRNA can substantially improve the anticancer activity of DOX in a triple negative breast cancer model.

Conclusion

In summary, we have designed a multifunctional porous silica-based nanoplatform for the codelivery of chemotherapeutic agents and siRNA to tumor tissue. The DOX loading capacity was substantially increased due to the implementation of a two-step loading procedure. The results demonstrate that this nanodelivery system is capable of siRNA protection, intracellular uptake, and lysosomal escape. Furthermore, the delivery system enables DOX and siRNA accumulation in tumor tissue following intravenous injection. The *in vivo* and *in vitro* results from this study demonstrate that gene silencing and cancer cell apoptosis was achieved. In particular, suppression of PKM2 expression was shown to sensitize breast cancer cells to DOX. In fact, PKM2 suppression reduced ATP levels in breast cancer cells, providing a potential clue to the mechanism involved in chemosensitization. Additionally, in an MDA-MB-231 orthotopic breast cancer model, the combination of DOX and PKM2 siRNA suppressed tumor growth to a greater extent than DOX alone. A complete understanding of the mechanism of PKM2 siRNA-induced chemosensitization could provide important insights for the optimization of this combination therapy. Taken together, this study lays the foundation for further development of porous silica-based nanoparticles for codelivery of chemotherapy and gene silencing agents.

Author contributions

Z. M. and H. S. developed the concept and supervised experiments. J. S., H. L. and J. W. prepared the manuscript with the assistance of Z. H., L. J. and M. F.; J. S., and H. L. fabricated CP-MSNP@DOX/PKM2 siRNA delivery system. J. S., H. L., W. Z., G. Z. and X. L. characterized the delivery system *in vitro*. J. S., H. L., C. M., J. W. and H. K. performed *in vivo* biological analyses. J.S. performed biostatistical analysis.

Conflict of interest

The authors have declared that no conflicts of interest exist.

Acknowledgements

This work was partially supported by the Ernest Cockrell Jr. Distinguished Endowed Chair (M. F.), US Department of Defense grant W81XWH-12-1-0414 (M. F.), National Institute of Health grants U54CA143837, U54CA151668 (M. F.) and 1R01CA193880-01A1 (H. S.), National Natural Science Foundation of China grants no. 21231007 and 21572282 (Z.-W. M.), the 973 Program no. 2014CB845604 and 2015CB856301 (Z.-W. M.), the Ministry of Education of China grant no. IRT1298 (Z.-W. M.), and supports from the Guangdong Provincial Department of Human Resources and Social Security and Technology (Z.-W. M.), and the Fundamental Research Funds for Central Universities (Z.-W. M.).

References

1 J. R. Heath and M. E. Davis, *Annu. Rev. Med.*, 2008, **59**, 251.
2 R. Sinha, G. J. Kim, S. Nie and D. M. Shin, *Mol. Cancer Ther.*, 2006, **5**, 1909–1917.
3 M. Ferrari, *Nat. Rev. Cancer*, 2005, **5**, 161–171.
4 D. Peer, J. M. Karp, S. Hong, O. C. Farokhzad, R. Margalit and R. Langer, *Nat. Nanotechnol.*, 2007, **2**, 751–760.
5 V. P. Torchilin, *Adv. Drug Delivery Rev.*, 2012, **64**, 302–315.
6 M. E. Davis and D. M. Shin, *Nat. Rev. Drug Discovery*, 2008, **7**, 771–782.
7 J. Wolfram, M. Zhu, Y. Yang, J. Shen, E. Gentile, D. Paolino, M. Fresta, G. Nie, C. Chen and H. Shen, *Curr. Drug Targets*, 2015, **16**, 1671–1681.
8 J. Wolfram, K. Suri, Y. Yang, J. Shen, C. Celia, M. Fresta, Y. Zhao, H. Shen and M. Ferrari, *Colloids Surf., B*, 2014, **114**, 294–300.
9 A. Suillerot, C. Gueye, M. Salerno, C. Loetchutinat, I. Fokt, M. Krawczyk, T. Kowalczyk and W. Priebe, *Curr. Med. Chem.*, 2001, **8**, 51–64.
10 R. K. Jain and T. Stylianopoulos, *Nat. Rev. Clin. Oncol.*, 2010, **7**, 653–664.
11 V. P. Torchilin, *Nat. Rev. Drug Discovery*, 2005, **4**, 145–160.
12 I. I. Slowing, B. G. Trewyn, S. Giri and V. S. Y. Lin, *Adv. Funct. Mater.*, 2007, **17**, 1225–1236.
13 X. Huang, P. K. Jain, I. H. El-Sayed and M. A. El-Sayed, *Nanomedicine*, 2007, **2**, 681–693.
14 J. Shen, H.-C. Kim, C. Mu, E. Gentile, J. Mai, J. Wolfram, L.-n. Ji, M. Ferrari, Z.-w. Mao and H. Shen, *Adv. Healthcare Mater.*, 2014, **3**, 1629–1637.
15 J. Shen, X. Wu, Y. Lee, J. Wolfram, Z. Yang, Z.-W. Mao, M. Ferrari and H. Shen, *J. Visualized Exp.*, 2015, e52075.
16 J. Shen, R. Xu, J. Mai, H.-C. Kim, X. Guo, G. Qin, Y. Yang, J. Wolfram, C. Mu, X. Xia, J. Gu, X. Liu, Z.-W. Mao, M. Ferrari and H. Shen, *ACS Nano*, 2013, **7**, 9867–9880.
17 N. Ž. Knežević and V. S.-Y. Lin, *Nanoscale*, 2013, **5**, 1544–1551.
18 F. Tang, L. Li and D. Chen, *Adv. Mater.*, 2012, **24**, 1504–1534.
19 Q. Zhang, F. Liu, K. T. Nguyen, X. Ma, X. Wang, B. Xing and Y. Zhao, *Adv. Funct. Mater.*, 2012, **22**, 5144–5156.
20 C.-H. Lee, L.-W. Lo, C.-Y. Mou and C.-S. Yang, *Adv. Funct. Mater.*, 2008, **18**, 3283–3292.
21 J. M. Rosenholm, C. Sahlgren and M. Lindén, *Nanoscale*, 2010, **2**, 1870–1883.
22 I. I. Slowing, J. L. Vivero-Escoto, C.-W. Wu and V. S. Y. Lin, *Adv. Drug Delivery Rev.*, 2008, **60**, 1278–1288.

23 J. Shen, H.-C. Kim, H. Su, F. Wang, J. Wolfram, D. Kirui, J. Mai, C. Mu, L.-N. Ji and Z.-W. Mao, *Theranostics*, 2014, **4**, 487–497.
24 T. Xia, M. Kovochich, M. Liong, H. Meng, S. Kabehie, S. George, J. I. Zink and A. E. Nel, *ACS Nano*, 2009, **3**, 3273–3286.
25 H. Meng, M. Liong, T. Xia, Z. Li, Z. Ji, J. I. Zink and A. E. Nel, *ACS Nano*, 2010, **4**, 4539–4550.
26 H. Meng, W. X. Mai, H. Zhang, M. Xue, T. Xia, S. Lin, X. Wang, Y. Zhao, Z. Ji, J. I. Zink and A. E. Nel, *ACS Nano*, 2013, **7**, 994–1005.
27 A. Popat, S. B. Hartono, F. Stahr, J. Liu, S. Z. Qiao and G. Q. M. Lu, *Nanoscale*, 2011, **3**, 2801–2818.
28 L. S. Jabr-Milane, L. E. van Vlerken, S. Yadav and M. M. Amiji, *Cancer Treat. Rev.*, 2008, **34**, 592–602.
29 B. Stewart and C. P. Wild, *World Cancer Rep*, 2016.
30 R. A. Cairns, I. S. Harris and T. W. Mak, *Nat. Rev. Cancer*, 2011, **11**, 85–95.
31 P. P. Hsu and D. M. Sabatini, *Cell*, 2008, **134**, 703–707.
32 Y. Zhao, E. B. Butler and M. Tan, *Cell Death Dis.*, 2013, **4**, e532.
33 M. M. Gottesman, T. Fojo and S. E. Bates, *Nat. Rev. Cancer*, 2002, **2**, 48–58.
34 K. A. Whitehead, R. Langer and D. G. Anderson, *Nat. Rev. Drug Discovery*, 2009, **8**, 129–138.
35 D. Castanotto and J. J. Rossi, *Nature*, 2009, **457**, 426–433.
36 H. R. Christofk, M. G. Vander Heiden, N. Wu, J. M. Asara and L. C. Cantley, *Nature*, 2008, **452**, 181–186.
37 M. Cortés-Cros, C. Hemmerlin, S. Ferretti, J. Zhang, J. S. Gounarides, H. Yin, A. Muller, A. Haberkorn, P. Chene and W. R. Sellers, *Proc. Natl. Acad. Sci. U. S. A.*, 2013, **110**, 489–494.
38 W. Luo and G. L. Semenza, *Trends Endocrinol. Metab.*, 2012, **23**, 560–566.
39 E. Martinez-Balibrea, C. Plasencia, A. Ginés, A. Martinez-Cardús, E. Musulén, R. Aguilera, J. L. Manzano, N. Neamati and A. Abad, *Mol. Cancer Ther.*, 2009, **8**, 771–778.
40 W. Yang and Z. Lu, *Cancer Lett.*, 2013, **339**, 153–158.
41 M. S. Goldberg and P. A. Sharp, *J. Exp. Med.*, 2012, **209**, 217–224.
42 C. E. DeSantis, S. A. Fedewa, A. Goding Sauer, J. L. Kramer, R. A. Smith and A. Jemal, *CA–Cancer J. Clin*, 2016, **66**, 31–42.
43 N. U. Lin, E. Claus, J. Sohl, A. R. Razzak, A. Arnaout and E. P. Winer, *Cancer*, 2008, **113**, 2638–2645.
44 M. J. Duffy, P. M. McGowan and J. Crown, *Int. J. Cancer*, 2012, **131**, 2471–2477.
45 J. Lu, M. Liong, J. I. Zink and F. Tamanoi, *Small*, 2007, **3**, 1341–1346.
46 S. Chono, S.-D. Li, C. C. Conwell and L. Huang, *J. Controlled Release*, 2008, **131**, 64–69.
47 N. Krall, F. Pretto, W. Decurtins, G. J. Bernardes, C. T. Supuran and D. Neri, *Angew. Chem., Int. Ed.*, 2014, **53**, 4231–4235.
48 T. Wei, C. Chen, J. Liu, C. Liu, P. Posocco, X. Liu, Q. Cheng, S. Huo, Z. Liang and M. Fermeglia, *Proc. Natl. Acad. Sci. U. S. A.*, 2015, **112**, 2978–2983.
49 J. Han, Q. Wang, Z. Zhang, T. Gong and X. Sun, *Small*, 2014, **10**, 524–535.
50 R. Molinaro, J. Wolfram, C. Federico, F. Cilurzo, L. Di Marzio, C. A. Ventura, M. Carafa, C. Celia and M. Fresta, *Expert Opin. Drug Delivery*, 2013, **10**, 1653–1668.
51 R. Salgia and A. T. Skarin, *J. Clin. Oncol.*, 1998, **16**, 1207–1217.
52 Y. Li, C.-P. Tan, W. Zhang, L. He, L.-N. Ji and Z.-W. Mao, *Biomaterials*, 2015, **39**, 95–104.
53 W.-N. Tian, L. D. Braunstein, J. Pang, K. M. Stuhlmeier, Q.-C. Xi, X. Tian and R. C. Stanton, *J. Biol. Chem.*, 1998, **273**, 10609–10617.
54 N. Khlebtsov and L. Dykman, *Chem. Soc. Rev.*, 2011, **40**, 1647–1671.
55 H. Kobayashi, R. Watanabe and P. L. Choyke, *Theranostics*, 2013, **4**, 81–89.
56 J. M. Li, Y. Y. Wang, M. X. Zhao, C. P. Tan, Y. Q. Li, X. Y. Le, L. N. Ji and Z. W. Mao, *Biomaterials*, 2012, **31**, 780–790.